REPORTS

- with those of steady hot spots for which spectroradiometry was possible. There was no evidence of any reaction without heating.
- 7. Angular-dispersive x-ray patterns were obtained at Stanford Synchrotron Radiation Laboratory beamline 10-2, using image plates with 17.038-keV monochromatic radiation. The patterns were analyzed as described by J. H. Nguyen and R. Jeanloz [Rev. Sci. Instrum. 64, 3456 (1993)]. The diffraction rings ascribed to diamond were narrow and uniform in intensity, indicating a randomly oriented polycrystalline reaction product and not diffraction from the single-crystal diamond anvils or chips coming off the anvils (which would instead yield individual diffraction spots or spotty diffraction rings). Additionally, there was no evidence after the experiments of any damage to the diamond anvils that could account for the evidence that diamond was present within the reacted samples.
- 8. Alkenes and alkynes, containing doubly and triply bonded carbons, are characterized by C-H stretching frequencies shifted upward by ~100 to 200 cm⁻¹ and another ~200 to 300 cm⁻¹ relative to those of singly bonded alkanes and CH₄ [D. C. Harris and M. D. Bertolucci, Symmetry and Spectroscopy (Dover Publications, New York, 1978)]. The vibrational frequencies depend on the types of bonds present and on the size and orientation of the molecule. The broad absorption band observed after reaction is therefore best interpreted as a superposition of bands from a mixture of differently sized and bonded hydrocarbons.
- 9. It is possible that hydrogen was present, but our Raman data near the H₂ vibrational mode at ~4250 cm⁻¹ [P. Loubeyre et al., Nature 383, 702 (1996)] were consistently too noisy to allow a definitive identification. Molecular hydrogen (H₂) exhibits no first-order infrared absorbtion, and free atomic hydrogen (H) has neither an infrared nor a Raman signature.
- 10. L. R. Benedetti and R. Jeanloz, in preparation. An x-ray beam collimated to a diameter of 20 μm was used to collect spatially resolved x-ray diffraction patterns at National Synchrotron Light Source beamline X17c. Energy dispersive patterns collected at $2\theta = 10^{\circ}$ documented an expanded unit cell for the part of the rhenium gasket adjacent to reaction products, and not for the part of the gasket next to unheated portions of the sample or in regions away from the sample. The observed shifts in lattice parameters, amounting to an expansion of as much as 2.6% $(\pm 0.2\%)$, are characteristic of rhenium hydride formation, with values of x up to 0.18 in ReH $_{\times}$ (20). Also, although iron hydride is formed more easily under pressure than is rhenium hydride (20, 21), we found no difference in results between samples contained in iron gaskets and those in rhenium gaskets.
- 11. J. C. Angus et al., Philos. Trans. R. Soc. London Ser. A 342, 195 (1993); C.-P. Klages, Appl. Phys. A (Solids Surf.) A56, 513 (1993). Diamond formed by chemical vapor deposition is extracted from CH₄ through a complex series of reactions that are chemically and structurally reliant on the presence of free hydrogen. If the process we observed is similar, then as hydrogen diffuses into the gasket, less hydrogen is available to sustain the diamond-forming reaction that we observed.
- 12. In addition to diamond, as described in the text, Raman spectroscopy of the opaque reaction product indicates the presence of varying amounts of another carbon phase that we infer to be amorphous carbon because it produces no identifiable x-ray diffraction line.
- 13. Sample regions with more ruby appeared to form more reaction products, which suggests that the ruby used for pressure calibration may provide nucleation sites. Also, Raman spectra of recovered material outside the diamond anvil cell indicate that the carbonaceous (opaque) reaction product was generally attached to ruby grains. Yoshimoto et al. similarly observed that Al₂O₃ provided nucleation sites for diamond growth (22). We did not observe any evidence of chemical reaction between the CH₄ and ruby, however, as the intensities of the fluorescence and x-ray diffraction lines of ruby were unchanged (within our resolution) before and after heating.

- B. R. Oppenheimer, S. R. Kulkarni, K. Matthews, M. H. van Kerkwijk, Astrophys. J. 502, 932 (1998); J. Liebert and W. B. Hubbard, Nature 400, 316 (1999).
- 15. An estimate of the energy that can be released from a dissociation reaction was made by calculating the gravitational energy for two models of Neptune's interior. The first is a three-layer model (rocky core, molecular "ice" layer, and hydrogen-helium atmosphere) by Hubbard (1), and the second is the same model except that the CH₄ in the "ice" layer is dissociated into diamond and hydrogen, with the diamond located at the bottom of the layer and the hydrogen at the top. The energy difference of 1.1 \times 10³³ I that is released in going from the first model to the second can be a significant source of internal energy for the planet. For comparison, Neptune is observed to radiate more than twice the energy it receives from the sun; the excess, 3.2 \times 10¹⁵ must be produced internally and corresponds to 0.45 \times 10³³ J over the 4.5-billion-year age of the solar system.
- 16. R. P. Butler et al., in preparation.
- H. K. Mao, P. M. Bell, K. J. Dunn, R. M. Chrenko, R. C. DeVries, Rev. Sci. Instrum. 50, 1002 (1979).
- 18. H. K. Mao et al., J. Appl. Phys. 49, 3276 (1978).
- R. Jeanloz and A. Kavner, *Philos. Trans. R. Soc. London Ser. A*, **354**, 1279 (1996); A. Kavner and R. Jeanloz, *J. Appl. Phys.* **83**, 7553 (1998).
- 20. T. Atou and J. V. Badding, J. Solid State Chem. 118, 299 (1995). Atou and Badding observed rhenium hydride with a stoichiometry up to x = 0.38 for ReH_x.
- 21. J. V. Badding and R. J. Hemley, *Science* **253**, 412 (1991).

- 22. M. Yoshimoto et al., Nature. 399, 340 (1999).
- 23. Infrared absorbance spectra (at 2 cm⁻¹ resolution) were recorded with a Bruker IFS66v Fourier-transform spectrometer using a Globar (mid-infrared) source, a calcium fluoride (CaF₂) beamsplitter, and a liquid N₂-cooled InSb detector.
- 24. R. Bini and G. Pratesi, Phys. Rev. B 55, 14800 (1997); Y. H. Wu, S. Sasaki, H. Shimizu, J. Raman Spectrosc. 26, 963 (1995). The CH₄ molecule has four normal modes of oscillation: a symmetric stretch, an antisymmetric stretch, a symmetric deformation, and an antisymmetric deformation. The vibrational frequencies of these modes are, respectively, 2917 cm⁻¹, 3019 cm⁻¹, 1534 cm⁻¹, and 1306 cm⁻¹ at ambient pressure and temperature, and they increase as pressure is raised (temperature is expected to have only a secondary effect).
- F. D. Bloss, An Introduction to the Methods of Optical Crystallography (Holt, Rinehart & Winston, San Francisco, 1961).
- 26. Raman spectra were excited with a Lexel 95 argonion laser tuned to a wavelength of 514.5 nm and were collected through a triple grating monochrometer/spectrograph (Spectra Pro 750) to a liquid N₂⁻ cooled charge-coupled device detector (Princeton Instruments ST 138, 100 × 1340 pixels). The laser was focused through a microscope, allowing 3 cm⁻¹ spectral resolution within a ~5-μm spot.
- 27. J. Michler et al., J. Appl. Phys. 83, 187 (1998).
- We thank P. Alivisatos, K. Jacobs, W. Panero, H. Scott, and S. Zatman for experimental support and helpful discussions. Supported by NSF and NASA.

10 June 1999; accepted 20 August 1999

Laminar Ceramics That Exhibit a Threshold Strength

M. P. Rao, A. J. Sánchez-Herencia, K. G. E. Beltz, R. M. McMeeking, F. F. Lange

Thin compressive layers within a laminar ceramic arrest large cracks (surface and internal) and produce a threshold strength. This phenomenon increases the damage tolerance of ceramics and will allow engineers to design reliable ceramic components for structural applications. The stress intensity factor derived for a crack sandwiched between two compressive layers suggests that the threshold strength is proportional to the residual compressive stress and the thickness of the compressive layer and is inversely proportional to the distance between the compressive layers. Laminates composed of thick alumina layers (605 \pm 11 micrometers) and thin mullite/alumina compressive layers (37 \pm 1.4 micrometers) fabricated for this study had a threshold strength of 482 \pm 20 megapascals, in fair agreement with the theory.

The strength of brittle materials, including ceramics and glasses, must be described by statistical parameters (such as those of Weibull) because they contain an unknown variety of cracks and cracklike flaws that are inadvertently introduced during processing and surface machining (1, 2). Typical flaws found at fracture origins include large voids produced by organic inclusions (such as a human hair) and inorganic inclusions (such as

- tinical in lifor-

¹Materials Department, ²Department of Mechanical and Environmental Engineering, University of California at Santa Barbara, Santa Barbara, CA 93106, USA.

*Present address: Instituto de Cerámica y Vidrio (CSIC), Arganda del Rey, 28500 Madrid, Spain. †To whom correspondence should be addressed.

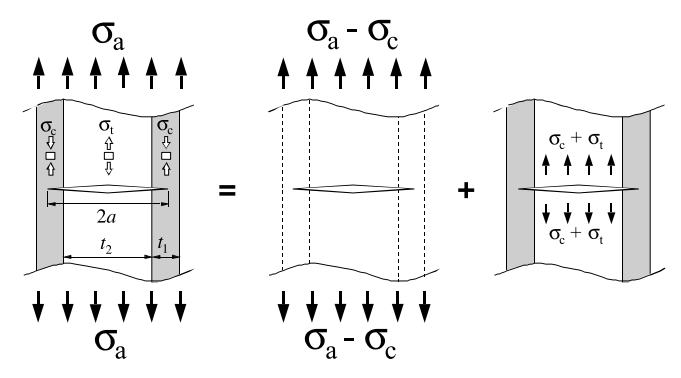
a dust particle or agglomerated particles). These flaws originate in the ceramic powders used to make the components. Failure from these types of flaws is generally not an issue in ductile materials, such as metals, because they exhibit plastic deformation that desensitizes the relation between small flaws and strength. Plastic deformation also absorbs work from the loading system to increase the metal's resistance to the extension of large cracks. However, the lack of plastic deformation causes the strength of ceramics to be inversely dependent on the size of very small cracks, which generally cannot be detected except by failure itself. For this reason, a specific ceramic component could exhibit a high probability of failure.

Proof testing must be used when performance outweighs consumer price sensitivity. The proof test is designed to emulate the thermal and mechanical stresses experienced by the component in severe service. The proof test defines a threshold stress, below which components are eliminated by failure before service. Eliminating heterogeneities from the ceramic powder that give rise to flaws is another approach to ensure reliability. One method to remove inclusions and agglomerates greater than a given size is to disperse the powder in a liquid and pass the slurry through a filter (1). If heterogeneities are not reintroduced in subsequent processing steps and if surface cracks introduced during machining are not a critical issue, filtration determines a threshold strength by defining the largest flaw that can be present in the powder and, thus, within the finished ceramic component (3). Methods for forming engineering shapes with filtered slurries are currently under development (4, 5).

Although others (6-9) have shown that residual compressive surface stresses will hinder the growth of surface cracks, Green et al. (10) have recently proposed that the compressive stress should be located at a specific distance beneath the surface. They suggest that the compressive stress will arrest surface cracks and result in higher failure stresses and reduced strength variability. However, compressive stresses, either at or just beneath the surface, will not effectively hinder internal cracks and flaws, nor can they produce a threshold strength. As discussed below, a threshold strength can only arise when thin compressive layers are placed throughout the body to interact with surface cracks and internal cracks and flaws.

A biaxial compressive stress arises within alternate layers of thickness t_1 , either surface or internal, when they are compressed in relation to a second set of alternate layers of thickness t_2 . A biaxial compressive strain mismatch ε arises when the t_1 layers either have a lower thermal expansion coefficient, undergo a volume increase due to a crystal-

Fig. 1. Schematic representation of the superimposed stress fields used to determine the stress intensity factor of the arrested crack. The left side shows a laminar ceramic composed of thin layers t₁ subject to residual compressive stresses σ and thick layers t_2 subject to tensile stresses σ_{t} , all of which were subjected to an applied tensile stress $\sigma_{\!\scriptscriptstyle a}.$ This laminate contains a slit crack of



length 2a that extends into the compressive layers. The stresses shown on the left can be produced by the superposition of the two stress states shown on the right.

lographic phase transformation, or increase their molar volume because of a chemical reaction. For a laminated plate composed of compressive layers t_1 , alternated between tensile layers t_2 , the biaxial stresses in both layers are given by (11)

$$\sigma_{1} = \varepsilon E'_{1} \left(1 + \frac{t_{1}E'_{1}}{t_{2}E'_{2}} \right)^{-1}$$

$$\sigma_{2} = -\sigma_{1} \frac{t_{1}}{t_{2}}$$
(1)

where $E_i' = E_i/(1 - \nu_i)$, E is Young's modulus, and ν is Poisson's ratio. Inspection of the two relations shows that thin compressive layers are desired because when $t_1/t_2 \rightarrow 0$, the compressive stress is maximized and the tensile stress diminishes to zero in the thicker layers.

The hypothesis that multiple thin compressive layers could result in a threshold strength had its genesis in experiments conducted to further understand crack bifurcation, that is, the 90° change in the direction of a crack as it enters and extends along the center line of a compressive layer (12, 13). In these experiments, a crack was observed to initiate and arrest between two compressive layers. This observation initiated a fracture mechanics analysis to determine the conditions for crack arrest and subsequent failure, and experiments to test the analysis.

The analysis assumes that a preexisting crack of length 2a spans the thick layer t_2 , sandwiched by the compressive thin layers of thickness t_1 , as shown on the left side of Fig. 1. The magnitude of the biaxial residual compressive stress within the thin layers is given by σ_{c} , and the opposing residual tensile stress within the thick layer is given by σ_t . The analysis determines the stress intensity factor for a crack of length 2a when it extends into the compressive layers $(t_2 \le 2a \le t_2 + 2t_1)$, under an applied stress σ_a that is parallel to the layers. The stress intensity factor is used to determine the applied stress, σ_{thr} , needed to extend the crack through the compressive layers to produce catastrophic failure.

The stress intensity factor K is determined by superimposing the two stress fields shown on the right side of Fig. 1, each applied to the same slit crack of length 2a and each with its own known stress intensity factor. The first is a tensile stress of magnitude $\sigma_a - \sigma_c$ applied to a cracked specimen that does not contain residual stresses. The stress intensity factor for this stress is given by the first term on the right-hand side of Eq. 2A. The second is a tensile stress of magnitude $\sigma_c + \sigma_t$, which is only applied across the thick layer (the portion of crack defined by t_2). Its stress intensity factor is given by the second term on the right side of Eq. 2A (14). The two superimposed stress fields sum to that shown on the left side of Fig. 1. The stress intensity factor for the two superimposed stress fields is thus given by

$$K = (\sigma_{a} - \sigma_{c}) \sqrt{\pi a}$$

$$+ (\sigma_{c} + \sigma_{t}) \sqrt{\pi a} \left[\frac{2}{\pi} \sin^{-1} \left(\frac{t_{2}}{2a} \right) \right] \qquad (2a)$$

Substituting $\sigma_t = \sigma_c t_1/t_2$ (from Eq. 1) and rearranging, one can better express the physical significance of the compressive layers as

$$K = \sigma_{a} \sqrt{\pi a}$$

$$+ \sigma_{c} \sqrt{\pi a} \left[\left(1 + \frac{t_{1}}{t_{2}} \right) \frac{2}{\pi} \sin^{-1} \left(\frac{t_{2}}{2a} \right) - 1 \right]$$
(2b)

The first term in Eq. 2B is the well-known stress intensity factor for a slit crack in an applied tensile field. The second term is always negative and therefore reduces the stress intensity factor when the crack extends into the compressive layers. Thus, the compressive layers increase the material's resistance to crack extension.

Because K decreases as the crack extends into the compressive layers, the maximum stress needed to cause the crack to "break" through the compressive layers occurs when $2a = t_2 + 2t_1$ and $K = K_c$, the critical stress intensity factor of the thin-layer material, a

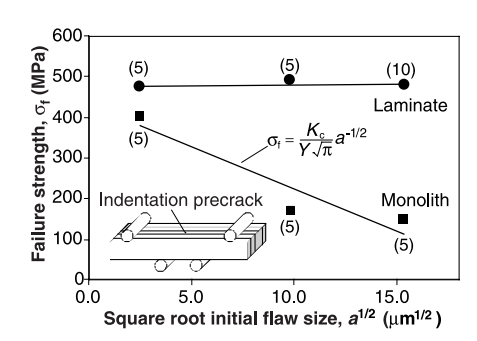


Fig. 2. Plot of the failure strength $\sigma_{\rm f}$ versus the square root of the initial flaw size a $^{1/2}$ for laminated and monolithic specimens, tested in the configuration shown in the inset. Numbers in parentheses indicate the number of specimens tested for that data point; SD for each was \leq 5%. Y, dimensionless constant.

REPORTS

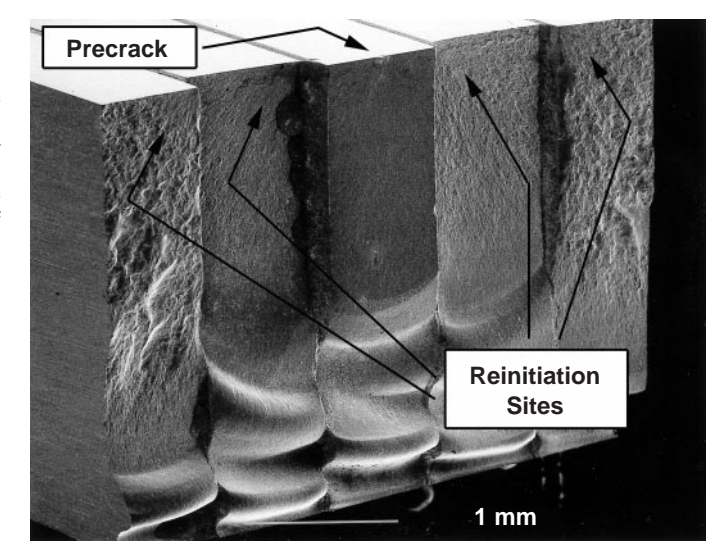
property that describes its intrinsic resistance to crack extension. Substituting these values into Eq. 2B and rearranging, one determines the largest stress needed to extend the crack through the compressive layers by

$$\sigma_{\text{thr}} = \frac{K_{c}}{\sqrt{\pi \frac{t_{2}}{2} \left(1 + \frac{2t_{1}}{t_{2}}\right)}} + \sigma_{c} \left[1 - \left(1 + \frac{t_{1}}{t_{2}}\right) \frac{2}{\pi} \sin^{-1} \left(\frac{1}{1 + \frac{2t_{1}}{t_{2}}}\right)\right]$$
(3)

Equation 3 shows that σ_{thr} increases with the fracture toughness of the thin-layer material $K_{\rm c}$, the magnitude of the compressive stress σ_c , and the thickness of the compressive layer t_1 . One can also show that if the initial crack length in the thick layer is less than t_2 and the stress needed to extend it is less than σ_{thr} , the crack will be arrested by the compressive layers. However, if the crack is very small and extends at a stress that is greater than σ_{thr} , it will extend though the compressive layers to cause catastrophic failure without being arrested. Thus, Eq. 3 defines a threshold stress σ_{thr} , below which the laminar body cannot fail when the tensile stress is applied parallel to the layers. This prediction has important implications. It allows an engineer to design structural components with the knowledge that the component will not fail below the threshold stress.

To test Eq. 3, we fabricated laminar plates that were composed of alternating layers of ${\rm Al_2O_3}$ (605 \pm 11 $\mu {\rm m}$ in thickness) and alternating layers of a mixture of 85 volume % mullite and 15 volume % ${\rm Al_2O_3}$ (85 M) (37 \pm 1.4 $\mu {\rm m}$ in thickness); these plate were fabricated with a sequential slip-casting technique described elsewhere (15). Monolithic ${\rm Al_2O_3}$ plates, without the compressive layers, were also fabricated, and all of the plates were den-

Fig. 3. A scanning electron micrograph of a typical fracture surface where fracture initiated, then arrested, in the central layer from the indentation crack. The top surface was the tensile face of the specimen.



sified by heating at 1550°C for 2 hours to achieve a relative density of ≥0.99. We estimated the residual compression within the thin 85 M layers, caused by differential thermal contraction during cooling to room temperature, to be 1.174 GPa by using the properties reported elsewhere (11, 12, 16, 17). This value was verified to be 1.181 ± 0.004 GPa by piezospectroscopic measurements, in which the stress-induced shift in the fluorescence spectra of trace Cr3+ impurities in alumina was used to measure residual stress (18). Flexural bars were cut from the plates, and one of the lateral surfaces was polished to facilitate the introduction of a Vickers indenter crack into either the central Al₂O₃ layer of each laminar specimen or into the center of the bar for the monolithic Al₂O₃ specimens.

In order to establish the invariance of the threshold strength with flaw size, specimens were precracked with indenter loads of 0.2, 2.5, and 5 kg. The lengths of the precracks were measured with selected specimens by making cellulose acetate replicas of the polished surfaces while they were under load (the stress was 125 MPa, well below the loads needed to initiate crack extension). The replica technique revealed precrack lengths of approximately 13, 193, and 470 µm, for the respective indenter loads. All of the specimens were tested in four-point flexural loading so that the indentation precrack was on the tensile surface and perpendicular to the direction of the applied tensile stress (see inset in Fig. 2). For several specimens, the load was removed after the indentation crack was observed to propagate and arrest at the bounding compressive layers. This initial crack extension and arrest occurred at stresses ranging from ≈150 MPa for the larger indentation cracks to ≈400 MPa for the smallest ones. Inspection with a scanning electron microscope revealed that the crack always arrested at or near the interface between the thick Al₂O₃ layer and the thin 85 M compressive layer. These specimens were then reloaded to failure to become part of the collective data.

Figure 2 shows that the failure stress of the laminates was relatively independent of the initial flaw size, and as expected, the strength of the monolithic alumina without the compressive layers was strongly dependent on the size of the indentation cracks. The range of threshold strength values was estimated to be between 363 to 394 MPa by substituting into Eq. 3 the value of the residual compression σ_c , the average values of t_1 and t_2 , and the range of K_c values reported for mullite (2 to 3 MPa m^{1/2}) (19). This range is lower but in fair agreement with the measured threshold strength of 482 \pm 20 MPa reported in Fig. 2.

Figure 3 shows a typical fracture surface of a laminar specimen. The markings on the fracture surface of the central alumina layer show that the precrack extended halfway down the central layer and arrested near the central axis of the flexural specimen, where the applied tensile stress diminishes to zero. Steps were produced when fracture progressed across the tensile surface into the other layers. These steps show that each compressive layer produced a limited amount of bifurcation (12, 13) as fracture proceeded across the specimen, layer by layer. With the exclusion of the center layer that contained the arrested crack, radiant markings (see arrows in Fig. 3) at the top corner (facing the center layer) showed that a new crack initiated in each layer during catastrophic fracture. The observation that catastrophic failure occurred by the reinitiation of a crack in each sequential layer shows that the crack did not fully propagate across the thin compressive layer as assumed for the stress intensity relation (Eq. 2B).

Our studies show that a ceramic laminate that contains thin compressive layers can be designed to have a threshold strength when a tensile stress is applied parallel to the layers, that is, a strength below which failure will not occur despite the presence of very large cracks. It is expected that the magnitude of the threshold strength will be proportional to the magnitude of the compressive stress and inversely proportional to the distance between the thin compressive layers (the thickness of the thick layers). Much larger threshold strengths are expected by reducing the thickness of the thick layers while maintaining the small thickness ratio of the two layers (that is, as $t_1/t_2 \rightarrow 0$). A theoretical analysis indicates that the layer thickness can be chosen to optimize the threshold stress in terms of material parameters (20). It is also expected that if a crack were introduced (for example, by an impact) to span one of the compressive layers, the threshold strength will be lower and defined by the distance between the next set of compressive layers.

In deriving Eq. 3, we assumed that the

REPORTS

arrested crack fully extends through the compressive layer in a straight path, whereas experimentally the crack is observed to bifurcate. Fracture in subsequent layers is reinitiated by a new crack and not by the original crack. Therefore, despite the fair agreement of the predicted and measured threshold strengths, it is still not certain that Eq. 3 accurately estimates the value of the threshold strength. Further experiments will be needed to fully understand this important phenomenon. In addition, the effect of the elastic moduli of the two materials, not considered here, is under consideration. However, it is expected that the phenomenon described here can be applied to other brittle materials, including glasses, many polymers, and some metals.

References and Notes

- 1. F. F. Lange, J. Am. Ceram. Soc. 72, 3 (1989).
- D. J. Green, Introduction to Mechanical Properties of Ceramics (Cambridge Univ. Press, Cambridge, 1998).
- 3. V. K. Pujari et al., Am. Ceram. Soc. Bull. 74, 86 (1995).
- G. V. Franks, B. V. Velamakanni, F. F. Lange, J. Am. Ceram. Soc. 78, 1324 (1995).
- 5. B. Yu and F. F. Lange, unpublished work.
- P. Honeyman-Colvin and F. F. Lange, J. Am. Ceram. Soc. 79, 1810 (1996).
- 7. F. F. Lange and B. I. Davis, ibid. 62, 629 (1979).
- 8. D. J. Green, J. Mater. Sci. 19, 2165 (1984).
- R. Lakshminarayanan, D. K. Shetty, R. A. Cutler, J. Am. Ceram. Soc. 79, 79 (1996).
- D. J. Green, R. Tandon, V. M. Sglavo, Science 283, 1295 (1999).
- C. Hillman, Z. Suo, F. F. Lange, J. Am. Ceram. Soc. 79, 2127 (1996).
- 12. M. Oechsner, C. Hillman, F. F. Lange, ibid., p. 1834.
- A. J. Sánchez-Herencia, C. Pascual, J. He, F. F. Lange, ibid. 82, 1512 (1999).
- 14. H. Tada, P. C. Paris, G. R. Irwin, The Stress Analysis of

- Cracks Handbook (Del Research, St. Louis, MO, ed. 2, 1985), p. 5.13.
- J. Requena, R. Moreno, J. S. Moya, J. Am. Ceram. Soc. 72, 1511 (1989).
- B. H. Mussler and M. W. Shafer, Am. Ceram. Soc. Bull. 63, 705 (1984).
- K. S. Mazdiyasni and L. M. Brown, J. Am. Ceram. Soc. 55, 548 (1972).
- 18. Q. Ma and D. R. Clarke, ibid. 77, 298 (1994).
- J. M. Rincon, G. Thomas, J. S. Moya, *ibid*. **69**, C29 (1986).
- 20. R. M. McMeeking and G. E. Beltz, unpublished work.
- 21. Supported by the Office of Naval Research under grant 442490-23074. A.J.S.-H. was supported by Ministerio de Educación y Cultura–Spain (grant PF96-0002872849) during his period as a visiting scientist at the University of California at Santa Barbara. We thank V. Tolpygo for his assistance in making the piezospectroscopic measurements used to verify the calculated value of the compressive stress within the thin layers.
 - 8 June 1999; accepted 19 August 1999

Enhanced Cortical Dopamine Output and Antipsychotic-like Effects of Raclopride by α_2 Adrenoceptor Blockade

Peter Hertel, Maria V. Fagerquist, Torgny H. Svensson*

Clozapine exerts superior clinical efficacy and markedly enhances cortical dopamine output compared with classical antipsychotic drugs. Here the α_2 adrenoceptor antagonist idazoxan was administered to rats alone or in combination with the $D_{2/3}$ dopamine receptor antagonist raclopride. Dopamine efflux in the medial prefrontal cortex and conditioned avoidance responding were analyzed. Idazoxan selectively potentiated the cortical output of dopamine and augmented the suppression of conditioned avoidance responding induced by raclopride. These results challenge basic assumptions underlying the dopamine hypothesis of schizophrenia and provide insight into clozapine's mode of action.

The dopamine hypothesis of schizophrenia rests basically upon the fact that all hitherto discovered antipsychotic drugs have been found to antagonize dopamine neurotransmission in brain (1). Positron emission tomography studies in humans reveal that classical antipsychotics in clinically effective doses yield about 70 to 80% D2 receptor occupancy in striatal tissue, which approaches the threshold for extrapyramidal side effects (2). In preclinical studies all antipsychotic drugs suppress conditioned avoidance responding (3, 4), a behavioral paradigm that has been attributed to drug effects on the subcortical, mesolimbic dopamine projection (5). The dopamine hypothesis of schizophrenia is, however, profoundly challenged by the atypical antipsychotic drug clozapine, which

Department of Physiology and Pharmacology, Section of Neuropsychopharmacology, Karolinska Institute, S-171 77 Stockholm, Sweden.

*To whom correspondence should be addressed: E-mail: torgny.svensson@fyfa.ki.se

shows significantly better efficacy than classical antipsychotics including an improved effect on negative symptoms (6), despite a lower D₂ receptor occupancy in brain [that is, \sim 45 to 50% (2)]. Clozapine accordingly has fewer extrapyramidal side effects (7). In contrast to classical antipsychotic drugs, clozapine causes a marked increase in dopamine output in the medial prefrontal cortex (8), an effect of considerable interest because of the role of prefrontal dopamine in cognitive functioning (9). Indeed, recent clinical evidence indicates that the degree of cognitive impairment largely determines treatment outcome in schizophrenia, in particular with regard to social functioning (10).

Clozapine has considerable affinity for α_2 adrenoceptors (11), and clinical trials demonstrate that adjuvant treatment with α_2 adrenoceptor antagonists may augment the clinical efficacy of classical D_2 receptor–blocking drugs (12). Accordingly, the α_2 adrenoceptor blocking effect of antipsychotic drugs, such as clozapine and risperidone, has been hy-

pothesized to be important for their clinical profiles (13).

We thus investigated the effects of combining a low dose of idazoxan, a specific α_2 adrenoceptor antagonist (14), with raclopride, a selective $D_{2/3}$ receptor antagonist (15), on dopamine output in the prefrontal cortex compared with subcortical regions of the brain. We also tested the effect of the drug combination on conditioned avoidance responding, a preclinical test with high predictive validity for a clinical antipsychotic effect (3, 4). We then tested the effect of the drug combination on catalepsy scores, a preclinical assessment of extrapyramidal side-effect liability (16).

Raclopride alone [0.05 mg per kilogram of body weight, subcutaneous injection (sc)] induced a marked increase in dopamine output as measured by microdialysis (17) in the nucleus accumbens and striatum, but caused only a small increase in the dopamine efflux in the medial prefrontal cortex (Fig. 1) (8). Idazoxan (1.5 mg/kg, sc) alone enhanced dopamine output in the medial prefrontal cortex and largely potentiated the raclopride-induced effects in the medial prefrontal cortex, whereas the subcortical areas remained unaffected (Fig. 1). This failure of idazoxan to augment the raclopride-induced increase in the subcortical areas is unlikely to be a ceiling effect, because a higher dose of raclopride (2.0 mg/kg, sc) further increased dopamine output in these brain regions (18). The regional selectivity of idazoxan on dopamine efflux is consistent with data from other, nonselective α_2 adrenoceptor antagonists (19) and may be indirectly related to its ability to facilitate cortical noradrenaline efflux (20). The noradrenaline transporter contributes to the clearance of dopamine from the extracellular compartment within the cortex (21). The concentrations of extracellular noradrenaline may affect cortical dopamine levels by competing for the same transporter.